Am J Cancer Res 2023;13(12):5901-5913
www.ajcr.us /ISSN:2156-6976/ajcr0153806

Original Article

CT-based radiomics nomogram for predicting visceral pleural invasion in peripheral T1-sized solid lung adenocarcinoma

Xiaoting Cai[1*], Ping Wang[2*], Huihui Zhou[3], Hao Guo[2], Xinyu Yang[1], Zhengjun Dai[4], Heng Ma[2]

[1]School of Medical Imaging, Binzhou Medical University, Yantai 264003, Shandong, China; [2]Department of Radiology, Yantai Yuhuangding Hospital, Qingdao University School of Medicine, Yantai 264001, Shandong, China; [3]Department of Pathology, Yantai Yuhuangding Hospital, Qingdao University School of Medicine, Yantai 264001, Shandong, China; [4]Department of Scientific Research, Huiying Medical Technology Co., Ltd., Beijing 100080, China. [*]Equal contributors.

Received October 7, 2023; Accepted November 27, 2023; Epub December 15, 2023; Published December 30, 2023

Abstract: The preoperative assessment of visceral pleural invasion (VPI) in patients with early lung adenocarcinoma is vital for surgical treatment. This study aims to develop and validate a CT-based radiomics nomogram to predict VPI in peripheral T1-sized solid lung adenocarcinoma. A total of 203 patients were selected as subjects, and were divided into a training cohort (n=141; scanned with Brilliance iCT256, Brilliance 64, Somatom Force, and Optima CT660) and a test cohort (n=62; scanned with Somatom Definition AS+). Radiomics characteristics were extracted from CT images. Variance thresholding, SelectKBest, and least absolute shrinkage and selection operator (LASSO) method were applied to determine optimum characteristics to construct the radiomic signature (radscore). After multivariate logistic regression analysis, a nomogram was structured regarding clinical factors, conventional CT features, and radscore. The nomogram property was tested based on its area under the curve (AUC). The nomogram based on the radscore and two conventional CT features (tumor pleura relationship and lymph node enlargement) showed high discrimination with an AUC of 0.877 (95% CI: 0.820-0.935) and 0.837 (95% CI: 0.737-0.937) in the training and test cohorts, respectively. The calibration curve and decision curve analysis showed good consistency and high clinical value of the nomogram. In conclusion, The CT-based radiomics nomogram was helpful in predicting VPI in peripheral T1-sized solid lung adenocarcinoma.

Keywords: Lung adenocarcinoma, visceral pleural invasion, radiomics, nomogram

Introduction

With the application of CT technology in lung cancer screening, an increasing number of early lung cancers have been found. Lung cancer can be split into small cell lung cancer and non-small cell lung cancer (NSCLC). The latter is more common, accounting for 85% of lung cancer [1]. Surgery is currently the dominant treatment for early NSCLC [1]. Visceral pleural invasion (VPI) of lung cancer, which is related to tumor recurrence, lymph node metastasis, and distant metastasis, is reportedly a poor prognosis factor for patients after surgery [2-5]. For T1-sized NSCLC, if VPI occurs, the tumor would upstage to T2a. Under the circumstances, lobectomy and more extensive lymph node dissection, rather than segmentectomy, are necessary during the operation [6, 7]. Therefore, an accurate assessment of VPI before surgery is essential for treatment decisions.

Puncture biopsy is an invasive procedure, and it assesses only a portion of the diseased tissue, not all lesions. CT becomes a vital auxiliary examination in the preoperative assessment of VPI [8]. Many CT features were found as risk factors for VPI, including pleural tags, tumor contact with pleura, tumor pleura contact length, tumor pleura distance, pleural indentation, tumor size, and lymph node enlargement [9-13]. Some clinical factors, including gender, age, and carcinoembryonic antigen (CEA) level, were also found to be risk factors for VPI in lung

cancer [10, 12, 13]. However, the diagnostic efficiency of VPI based on conventional CT features and clinical factors is not high. Ahn et al. [9] found that the sensitivity of CT features in VPI diagnosis was only 0.25 for T1-sized peripheral adenocarcinomas. Iizuka et al. constructed a risk-score model based on clinical factors and conventional CT features for the VPI prediction of NSCLC, and the area under the curve (AUC) of their model was 0.68 [12]. Thus, it is necessary to develop a new method for enhancing the diagnostic precision of VPI.

Radiomics has become a research hotspot because it can high-dimensionally extract massive characteristics from images to quantify the intrinsic heterogeneity of lesions [14]. Now, it is extensively applied in the diagnosis, pathological subtype classification, and prognosis prediction of lung cancer [15, 16]. However, only a few studies have focused on VPI prediction by radiomics. Zuo et al. constructed a nomogram containing texture features to predict the VPI of lung adenocarcinoma, and the model exhibits high classification performance, with a C-index of 0.864 [17]. Similarly, Wei et al. constructed a nomogram combining CT texture features and conventional CT features for the VPI prediction of T1-sized NSCLC. Their model showed a good classification property, with an AUC of 0.894 [18]. It is suggested that radiomics combined with conventional CT features can improve the diagnostic efficacy of the VPI of lung cancer compared with single conventional CT features.

Adenocarcinoma, which accounts for about half of NSCLCs, is very common in lung cancer [19]. Adenocarcinoma is mainly located peripherally and close to the pleura, so VPI can easily occur. Based on CT density, adenocarcinoma can be split into pure ground glass nodules (pGGNs), part solid, and pure solid nodules. Given the heterogeneity of adenocarcinoma, the probability of VPI and the risk factors of VPI vary among different substyles on CT. Several studies have confirmed that pGGNs do not or only rarely occur VPI, and with the increase in solid proportion, the malignant degree and the probability of VPI of adenocarcinomas increase [9, 20, 21]. Some studies have proven that VPI is a poor prognostic factor only for pure solid tumors [22, 23]. However, few studies have focused on VPI in pure solid lung adenocarcinoma [21], and no study using the radiomics method for VPI prediction in pure solid lung adenocarcinoma has been reported to our knowledge. Accordingly, the present study selected T1-sized pure solid adenocarcinoma as the research object and explored the diagnostic performance of radiomics combined with conventional CT features and clinical factors for VPI prediction.

Materials and methods

Patients

This study was approved by the Institutional Ethics Committee of Yantai Yuhuangding Hospital, and informed consent was waived. All patients were collected from Yantai Yuhuangding Hospital. The manuscript was prepared and revised according to the TRIPOD checklist of items (Supplementary File 1). A total of 831 cases who underwent chest CT scans before operations and were confirmed with lung cancer by postoperative pathology from May 2019 to Feb 2021 were reviewed retrospectively. The inclusion criteria: (1) patients with tumor confirmed as adenocarcinoma by pathology, (2) patients whose VPI status was confirmed by pathology, (3) patients whose CT results suggested pure solid tumor, (4) patients with tumor smaller than or equal to 3.0 cm in diameter, (5) patients with tumor located away from the segmental bronchi, (6) patients who received operation within two weeks after CT scans, and (7) patients with comprehensive and standardized medical records, encompassing the present and past medical history, as well as the findings from preoperative laboratory and imaging examinations. The exclusion criteria: (1) patients accepted neoadjuvant treatment before CT scans, and (2) patients with poor imaging quality due to respiratory or movement artifacts. The study flow chart is shown in **Figure 2**.

Pathological VPI evaluation

All specimens were evaluated by an experienced pathologist. According to the TNM Classification for Lung and Pleural Tumors (Ninth edition) [24], the reference standards of VPI were as follows: PL0, tumor did not invade the elastic fibers; PL1, tumor invaded the elastic fibers; and PL2, tumor further invaded the visceral pleural surface. When the hematoxylin

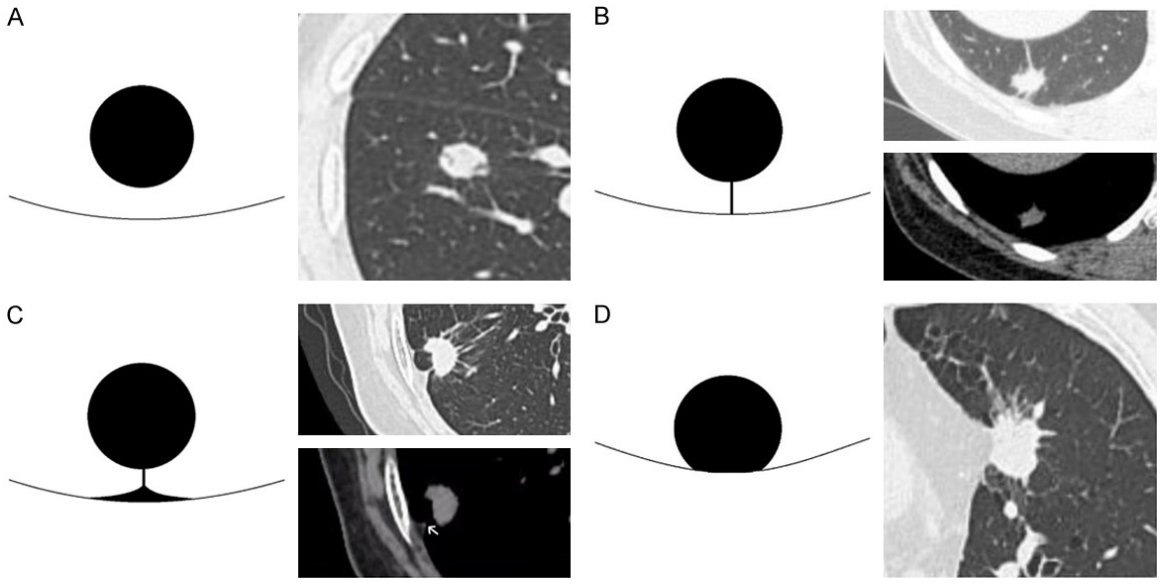

Figure 1. Pattern diagrams and CT images of tumor pleura relationships (I-IV). A. Type I, the tumor was unrelated to the pleura. B. Type II, the tumor was not contacted with the pleura directly, but the linear pleural tag was visible. C. Type III, the tumor was not contacted with the pleura directly, but the linear pleural tag with the density of soft tissue on the pleural side was visible (arrow). D. Type IV, the tumor was contacted with the pleura directly.

and eosin (H&E) stain could not determine whether the elastic fibers were invaded, special elastic staining was used for further evaluation [25]. PL0 was classified as VPI negative, and PL1 and PL2 were classified as VPI positive.

CT scanning protocol

All research subjects accepted chest CT scanning on the following devices: Brilliance iCT256 or Brilliance 64 (Philips Medical), Somatom Force or Somatom Definition AS+ (Siemens Medical), and Optima CT660 (GE Medical). The CT parameters were as follows: tube voltage, 80-120 kV; tube current, 120-250 mA; reconstruction slice thickness, 1.25 or 1 mm; matrix, 512 × 512; field of view, 500 mm; lung window width/level, 1600/-500 HU; and mediastinum window width/level, 300/45 HU.

Data extraction

We collected data including baseline clinical factors, conventional CT features, and radiomic characteristics.

Baseline clinical factors, including sex, age, smoking history, history of other malignancy, family history of lung cancer, tumor location and tumor markers of lung cancer, were derived from medical record systems. Tumor markers included CEA, neuron-specific enolase (NSE), cytokeratin 19 fragment antigen 21-1 (CYFRA21-1), and squamous cell carcinoma antigen (SCCA) level.

Two radiologists (with abundant experience in chest disease imaging diagnosis) assessed the conventional CT features of each case. The conventional CT features included tumor pleura relationship and other conventional CT features. According to previous studies [11, 13], we divided tumor pleura relationship into four types: type I, the tumor was unrelated to the pleura; type II, the tumor was not directly contacted with the pleura, but the linear pleural tag was visible; type III, the tumor was not directly contacted with the pleura, but the linear pleural tag with density of soft tissue on the pleural side was visible; and type IV, the tumor was contacted with the pleura directly (**Figure 1**). Other relationships between tumor and pleura included the following: (1) pleural indentation (absent or present); (2) tumor pleura contact length (the maximum contact length measured on axial, sagittal, or coronal mediastinum window images); and (3) tumor pleura distance (the shortest distance measured on axial, sagittal, or coronal mediastinum window images). Other conventional CT features included the following: (1) tumor size (the longest diameter

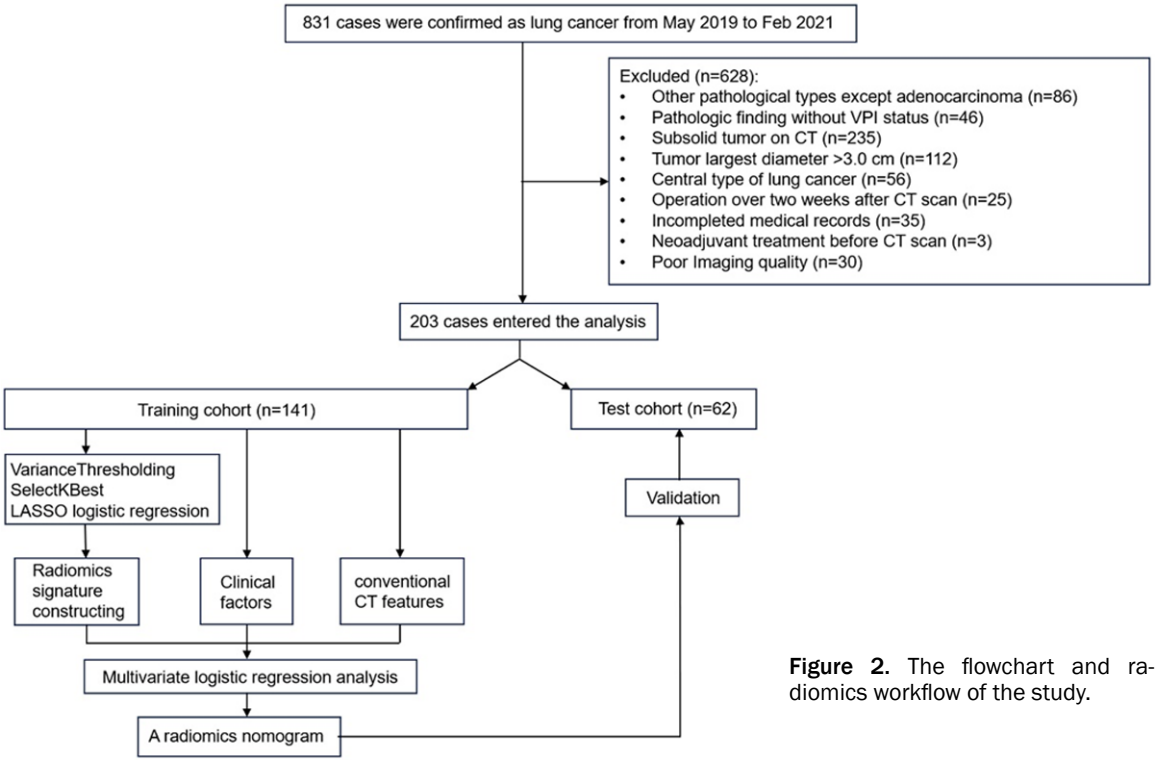

Figure 2. The flowchart and radiomics workflow of the study.

measured on axial, sagittal, or coronal lung window images); (2) shape (round/oval or irregular); (3) lobulation (absent or present); (4) tumor-lung interface (smooth or rough); (5) spiculation (absent or present); (6) bronchial cut-off sign (absent or present); (7) CT value; (8) vacuole (absent or present); (9) lymph node enlargement (the shortest diameter of the thoracic lymph node more than 1 cm on axial CT; absent or present); and (10) vascular convergence (absent or present).

The radiomic workflow is shown in **Figure 2**. The RadCloud platform (Huiying Medical Technology Co., Ltd., http://radcloud.cn/) was employed to segment tumors and extract radiomic characteristics. Two radiologists with 7 (reader A) and 14 (reader B) years of experience in chest disease imaging diagnosis manually segmented the volume of interest. Initially, they randomly segmented 50 nodules to extract characteristics to verify interobserver reproducibility. Then, reader A repeated the identical procedure half a month later to verify intraobserver reproducibility. Intraclass correlation coefficients (ICCs) were applied to assess the consistency of characteristic extraction regarding intraobserver and interobserver reproducibility. Characteristics with ICC > 0.75 were retained for further analysis. Reader A continually segmented residual nodules. A total of 1409 radiomics characteristics were extracted from each tumor's CT images, including texture, first-order, and high-order characteristics.

Model development and validation

Three methods were applied to determine the optimum radiomic characteristics from the training cohort. First, Variance Thresholding was performed to eliminate low variance characteristics. Then, SelectKBest was used to retain the invariant value. Finally, the least absolute shrinkage and selection operator (LASSO) was applied to ascertain optimum characteristics. The radiomics signature (radscore), which can provide a linear combination using the optimum characteristics to quantify radiomics signature, was calculated. The radscore performance was verified according to the receiver operating characteristic (ROC) curve.

Multivariate logistic regression analysis was used to acquire independent predictors for VPI in conventional CT features, clinical factors, and radscore between VPI positive and nega-

tive groups. A radiomics nomogram that could quantitatively and individually predict VPI was constructed on this basis. The ROC curve was used to verify the property of the nomogram. The calibration curve was applied to assess the classification precision of the prediction probability between observations. Decision curve analysis (DCA) was conducted to test the clinical applicability of the nomogram.

We also constructed a clinical model to compare with the traditional clinical VPI prediction method. Univariate and multivariate logistic regression analyses were performed to determine the independent risk factors among all clinical factors and conventional CT features. The clinical model was constructed based on independent risk factors.

Statistical analysis

Statistical analyses were carried out using R and SPSS software. Kappa statistics for categorical variables and ICC for quantitative variables were applied to measure the interobserver and intraobserver evaluation consistency, with ICC > 0.75 indicating a good consistency. Cases were classified into the training and test cohorts for building and validating models. Differences in variables between VPI positive and negative groups were computed based on the t-test or Wilcoxon rank-sum test for quantitative variables and Fisher exact or chi-square test for categorical variables. AUCs were calculated to assess each model property (clinical model, radiomic model, and nomogram) and compared by the DeLong test. $P < 0.05$ indicates statistical significance.

Results

Patients' characteristics and conventional CT features

A total of 203 cases were included and assigned to the training cohort (n=141; scanned with Brilliance iCT256, Brilliance 64, Somatom Force, and Optima CT660) and the test cohort (n=62; scanned with Somatom Definition AS+). Among the 203 patients, 55 (27.1%) were confirmed as VPI positive, and 148 cases (72.9%) as VPI negative. In the training cohort, 38 cases (27.0%) were confirmed as VPI positive, and 103 cases (73.0%) as VPI negative. For the test cohort, 17 cases (27.4%) were confirmed as VPI positive, and 45 cases (72.6%) as VPI negative.

The basic clinical factors and conventional CT features of patients are listed in **Table 1**. No significant differences were found in the baseline characteristics between the training and test cohorts. A good interobserver reproducibility existed between the two radiologists in assessing traditional CT features (ICC=0.849-0.986). Univariate analysis showed that types III and IV tumor pleura relationship were more likely to lead to VPI than types I and II. However, no noticeable difference existed between types III and IV, and no noticeable difference existed between types I and II. Therefore, we further divided the tumor pleura relationship into Group A (type I + II) and Group B (type III + IV). The chi-square test showed that Group B was more likely to lead to VPI than Group A ($P < 0.05$).

Radiomics characteristic selection and radiomics signature construction

A total of 1234 characteristics (ICC > 0.75) were retained after Variance Thresholding from initial 1409 radiomics characteristics. Then, 427 characteristics were retained with SelectKBest. Finally, 11 characteristics were selected as the optimum characteristics after LASSO to construct a relevant radiomics signature (radscore) (Supplementary File 2) (**Figure 3**). The radscore statistically differed between the VPI positive and negative groups ($P < 0.05$) (**Figure 4**).

Nomogram construction

Multivariate logistic regression was conducted between the VPI positive and negative groups among all variables (conventional CT features, clinical factors, and radscore). Finally, two conventional CT features (types III and IV tumor pleura relationship and lymph node enlargement) and the radscore were ascertained as independent VPI predictors. A radiomics nomogram based on these critical predictors was constructed (**Figure 5**).

Performance comparison of the three models

The AUCs of the clinical model, radiomics model, and nomogram (combined model) were 0.696, 0.819, and 0.877 in the training cohort

Table 1. Patient characteristics and conventional CT features in the training and test cohorts

Items	Training cohort (n=141)			Test cohort (n=62)		
	VPI(-) n=103	VPI(+) n=38	*P*	VPI(-) n=45	VPI(+) n=17	*P*
Age (y)	60.34±8.55	62.89±9.75	0.132	62 (57, 67)	59 (49, 67)	0.492
Sex			0.113			0.429
Male	45 (44)	23 (61)		17 (38)	9 (53)	
Female	58 (56)	15 (39)		28 (62)	8 (47)	
Location			0.966			0.960
RUL	21 (20)	9 (24)		15 (33)	5 (29)	
RML	9 (9)	3 (8)		3 (7)	1 (6)	
RLL	26 (25)	11 (29)		9 (20)	5 (29)	
LUL	26 (25)	9 (24)		5 (11)	2 (12)	
LLL	21 (20)	6 (16)		13 (29)	4 (24)	
CEA (ng/ml)			0.765			0.073
< 5	88 (85)	31 (82)		39 (87)	11 (65)	
≥ 5	15 (15)	7 (18)		6 (13)	6 (35)	
NSE (ng/ml)			0.947			1
< 17.5	81 (79)	29 (76)		37 (82)	14 (82)	
≥ 17.5	22 (21)	9 (24)		8 (18)	3 (18)	
CYFRA21-1 (ng/ml)			0.471			1
< 3.3	81 (79)	27 (71)		33 (73)	12 (71)	
≥ 3.3	22 (21)	11 (29)		17 (27)	5 (29)	
SCCA (ng/ml)			1			0.476
< 2	103 (100.0)	38 (100)		44 (98)	16 (94)	
≥ 2	0 (0)	0 (0)		1 (2)	1 (6)	
Smoking history			0.691			1
No	81 (79)	28 (74)		33 (73)	13 (76)	
Yes	22 (21)	10 (26)		12 (27)	4 (24)	
Family history of lung cancer			1			0.568
No	99 (96)	37 (97)		41 (91)	17 (100)	
Yes	4 (4)	1 (3)		4 (9)	0 (0)	
History of other malignancy			1			1
No	95 (92)	36 (95)		40 (89)	15 (88)	
Yes	8 (8)	2 (5)		5 (11)	2 (12)	
Tumor pleura relationship			0.002			< 0.001
I	14 (14)	0 (0)		9 (20)	0 (0.0)	
II	29 (28)	4 (11)		16 (36)	0 (0.0)	
III	11 (11)	7 (18)		2 (4)	2 (12)	
IV	49 (48)	27 (71)		18 (40)	15 (88)	

Tumor pleura relationship (Binary classification)			0.001			< 0.001
I + II	43 (42)	4 (11)		25 (56)	0 (0)	
III + IV	60 (58)	34 (89)		20 (44)	17 (100)	
Pleural indentation			0.020			0.131
Absent	65 (63)	15 (39)		29 (64)	7 (41)	
Present	38 (37)	23 (61)		16 (36)	10 (59)	
Tumor pleura contact length (mm)	0 (0, 10.3)	10.87 (0, 15.18)	0.003	0 (0, 7.64)	12.84 (8.57, 22,38)	< 0.001
Tumor pleura distance (mm)	1.01 (0, 5.56)	0 (0, 2.05)	0.003	1.33 (0, 4.69)	0 (0, 0)	0.003
Tumor size (mm)	16.35 (12.43, 22.25)	21.25 (17.62, 25.72)	< 0.001	15.54 (11.18, 20.93)	24.04 (14.17, 27.23)	0.031
Shape			1			0.712
Round/oval	90 (87)	33 (87)		36 (80)	15 (88)	
Irregular	13 (13)	5 (13)		9 (20)	2 (12)	
Lobulation			0.928			0.740
Absent	24 (23)	6 (16)		10 (22)	5 (29)	
Present	79 (77)	32 (84)		35 (78)	12 (71)	
Tumor-lung interface			0.235			0.242
Smooth	13 (13)	5 (13)		5 (11)	4 (24)	
Rough	90 (87)	33 (87)		40 (89)	13 (76)	
Spiculation			0.024			0.992
Absent	32 (31)	4 (11)		14 (31)	6 (35)	
Present	71 (69)	34 (89)		31 (69)	11 (65)	
Bronchial cut-off sign			0.712			0.591
Absent	65 (63)	22 (58)		29 (64)	9 (53)	
Present	38 (37)	16 (42)		16 (36)	8 (47)	
CT value (Hu)	30.27 (15.39, 39.98)	37.65 (23.51, 42.28)	0.025	28.62 (9.78, 44.29)	28.00 (18.00, 37.32)	0.067
Vacuole			0.623			0.432
Absent	64 (62)	26 (68)		25 (56)	12 (71)	
Present	39 (38)	12 (32)		20 (44)	5 (29)	
Lymph node enlargement			0.009			0.440
Absent	99 (96)	31 (82)		39 (87)	13 (76)	
Present	4 (4)	7 (18)		6 (13)	4 (24)	
Vascular convergence			0.006			1
Absent	37 (36)	4 (11)		16 (36)	6 (35)	
Present	66 (64)	34 (89)		29 (64)	11 (65)	

RUL = right upper lobe; RML = right middle lobe; RLL = right lower lobe; LUL = left upper lobe; LLL = left lower lobe; CEA = carcinoembryonic antigen; NSE = neuron-specific enolase; CYFRA21-1 = cytokeratin 19 fragment antigen 21-1; SCCA = squamous cell carcinoma antigen.

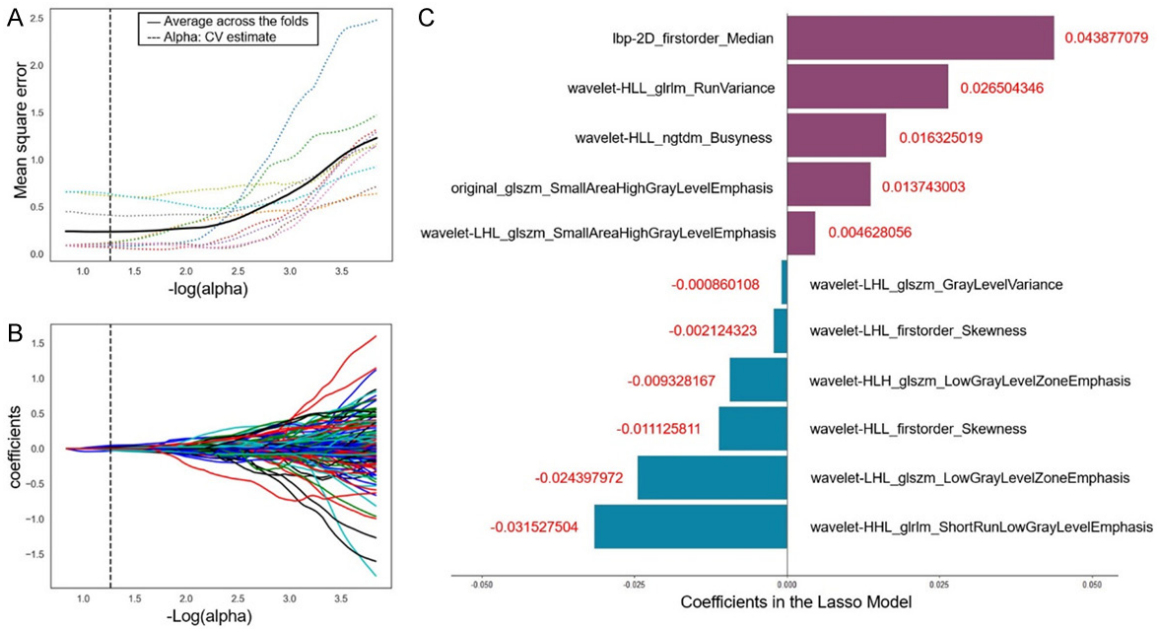

Figure 3. Radiomics characteristics selection using LASSO logistic regression. A. Cross-validation curve. Choice of optimum log lambda (λ) in the lasso model. B. LASSO coefficient profiles radiomics characteristics. Optimum λ (the dotted vertical line) selected 11 non-zero coefficients. C. The histogram shows the 11 selected optimum radiomics characteristics' contribution to the signature construction.

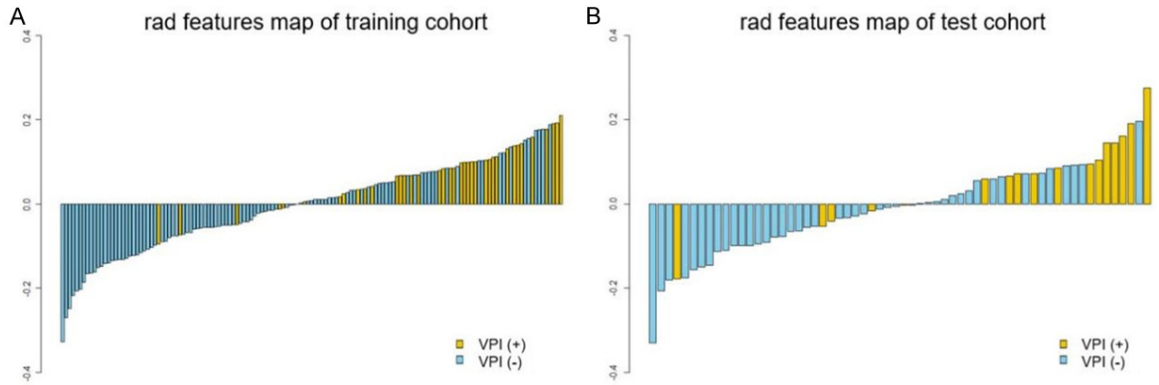

Figure 4. Radscore of patients in the training (A) and test (B) cohorts. Yellow indicates VPI positive patient and blue indicates VPI negative patient. Radscore, which was calculated by 11 optimum radiomic characteristics for each patient, showed significant differences between VPI positive and negative patients in both the training and test cohorts ($P < 0.05$).

and 0.775, 0.771, and 0.837 in the test cohort, respectively (**Figure 6**). The results showed that the nomogram had better VPI discrimination than the radiomics model and the clinical model ($P < 0.05$). The accuracy, sensitivity, and specificity of the three models are shown in **Table 2**.

The calibration curve of the nomogram reflected a high consistency between the predictions and the actual observed values (**Figure 7**). The DCA manifested that the net benefit level of the nomogram was superior to the other two models, with threshold probability between 0 to 34%, 38% to 59% and 63% to 96% (**Figure 8**).

Discussion

This research established a CT-based radiomics nomogram to predict VPI in T1-sized

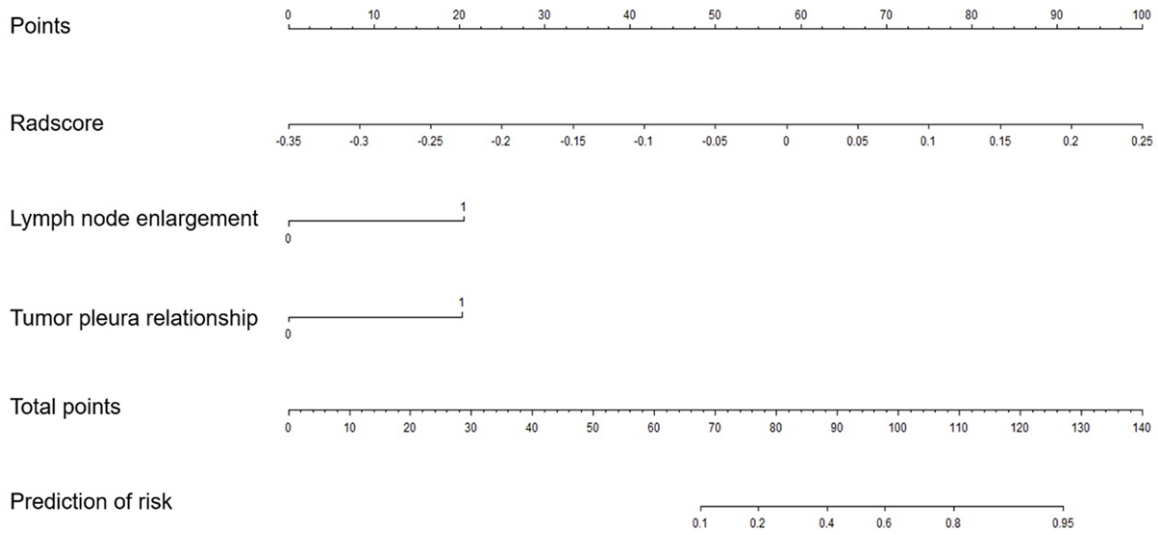

Figure 5. A radiomics nomogram based on radscore and two conventional CT features (tumor pleura relationship and lymph node enlargement) for the prediction of VPI in the training cohort.

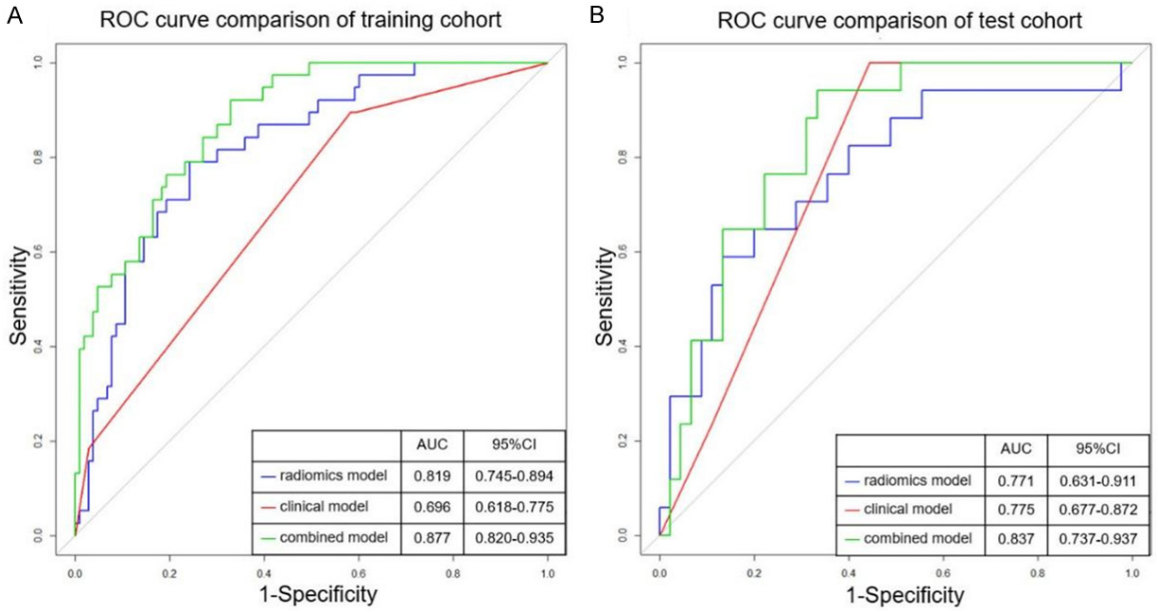

Figure 6. Comparison of the performance of three models. Receiver operating characteristic (ROC) curves of clinical model, radiomics model, and combined model (radiomics nomogram) in the training (A) and test (B) cohorts.

Table 2. Performances of the Three Models on Predicting VPI

Models		AUC	ACC	SEN	SPE
Radiomics nomogram	Training cohort	0.877	0.752	0.789	0.738
	Test cohort	0.837	0.758	0.706	0.778
Clinical model	Training cohort	0.696	0.759	0.184	0.971
	Test cohort	0.775	0.710	0.235	0.889
Radiomics model	Training cohort	0.819	0.723	0.816	0.689
	Test cohort	0.771	0.758	0.647	0.800

VPI = visceral pleural invasion; AUC = area under the curve; ACC = accuracy; SEN = sensitivity; SPE = specificity.

solid lung adenocarcinoma. This nomogram combining radscore and two CT features (tumor pleura relationship and lymph node enlargement) achieved good prediction ability for VPI. Furthermore, it exhibited high precision and application value in terms of its calibration curves and DCA.

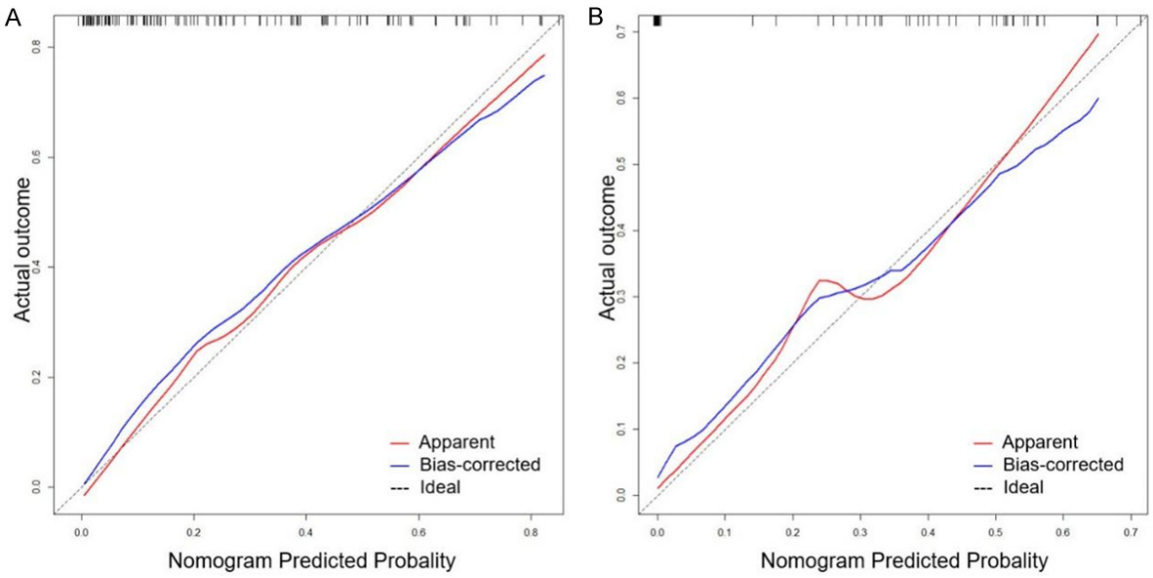

Figure 7. The calibration curves of the radiomics nomogram were used to evaluate the consistency between prediction probability and observations in the training (A) and test (B) cohorts.

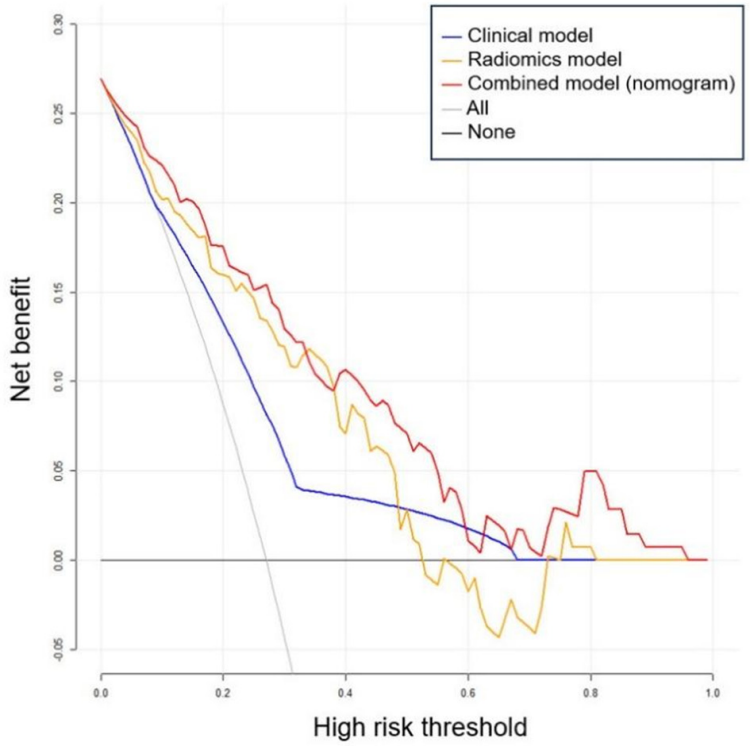

Figure 8. Decision curve analysis (DCA) for the prediction of VPI in peripheral T1-sized solid lung adenocarcinoma for each model. The X-axis represents the threshold probability, and the Y-axis represents the net benefit. The DCAs showed that the net benefits of the nomogram (red line) were superior to those of the radiomics model (yellow line) and the clinical model (blue line) between 0 to 34%, 38% to 59% and 63% to 96%.

Referring to previous studies [11, 13], we divided the tumor pleura relationship into four types. Results showed that types III and IV tumor pleura relationships were independent risk factors for VPI in T1-sized solid adenocarcinoma. None of type I and only 8.2% of type II tumor pleura relationship led to VPI, consistent with previous findings [11]. About 40.9% of type III tumor pleura relationship led to VPI, similar to Hsu et al.'s study [11]. However, the study of Hsu et al. did not involve type IV, and we found that type IV tumor pleura relationship was also a risk factor for VPI, with 38.5% VPI incidence for T1-sized solid adenocarcinoma. Zhao et al. found no pGGNs occurred VPI after microscopically observing, even in pGGNs with pleural attachment [20]. Considering the heterogeneity of adenocarcinoma, the probability of VPI and its risk factors vary among the different sub-

styles of adenocarcinoma according to CT density [21]. Other relationships between tumor and pleura such as, pleural indentation and tumor pleura contact length, have been reported as risk factors for VPI among different studies [10, 12, 13, 21]. Our univariate analysis found that tumor pleura contact length, tumor pleura distance, and pleural indentation statistically varied between the VPI positive and negative groups in peripheral T1-sized solid adenocarcinoma, but no statistical differences were identified in multivariate logistic analysis. The discrepancy may be due to the different study objects and included factors among our study and previous ones [10, 12, 13, 21].

Our work demonstrated that lymph node enlargement on CT was a risk factor for VPI in peripheral T1-sized solid adenocarcinoma, similar to previous studies [12]. Pleurae are rich in communicating lymphatic networks that drain into the mediastinal lymph nodes [12]. Accordingly, tumor cells can easily metastasize to the mediastinum lymph nodes through the lymphatic networks when VPI occurs. Previous research has shown that VPI is concerned with mediastinal lymph node metastasis [10], and lymph node enlargement on CT is a hazard for metastasis in solid lung cancer [26]. Thus, lymph node enlargement on CT also becomes an independent risk factor for VPI. In univariate analysis, our study showed statistical differences in tumor size, CT value, vascular convergence, and spiculation between the VPI positive and negative groups ($P < 0.05$). However, they were not identified as independent risk factors for VPI in peripheral T1-sized solid adenocarcinoma in multivariate analysis.

Radiomics can high-dimensionally extract massive invisible characteristics from CT images to quantify the intrinsic heterogeneity of tumors [13]. Up to 1409 radiomics characteristics were extracted from CT images of each tumor in our study. After assessing intraobserver and interobserver reproducibility, Variance Thresholding, SelectKBest, and LASSO selection, 11 optimum radiomics characteristics were retained to calculate radscore. The nomogram (combined model) combining radscore and two CT features (tumor pleura relationship and lymph node enlargement) showed superior performance for VPI prediction than the radiomics model and clinical model ($P < 0.05$). Our study confirmed that radiomic characteristics are essential supplements to conventional CT features for VPI prediction in peripheral T1-sized solid adenocarcinoma. The 11 quantitative radiomics characteristics finally retained were all high-order characteristics originating from primary images. Therefore, the high-order statistical characteristics were more valuable for VPI prediction in peripheral T1-sized solid adenocarcinoma than the other features. Wei et al. constructed a joint VPI prediction model combining CT texture features and conventional CT features [18]. The predictive performance of their model is higher than ours (AUC: 0.894 vs. 0.837). However, their study object was NSCLC, which included a variety of lung cancer pathological types. Zuo et al. constructed a nomogram containing texture features to predict the VPI of lung adenocarcinoma [17]. Zha et al. constructed a nomogram combining radiomics and CT features for the VPI prediction of lung adenocarcinoma [27]. Their models exhibited high classification property, with a C-index of 0.864 and AUC of 0.89, which are slightly higher than ours. Unlike our study objects of pure solid adenocarcinomas, Zuo et al.'s study objects included subsolid and solid adenocarcinomas. Zha et al.'s study objects were part solid and pure solid adenocarcinomas. Although we used the semblable research method, most clinical predictive factors and radiomics characteristics of the models varied between our studies. This finding indicated the heterogeneity of the adenocarcinoma among different subgroups on CT.

Previous studies have confirmed that the prognosis differs among various subgroups of adenocarcinoma based on CT [22, 28]. The prognosis of adenocarcinoma with ground glass component is better than that of pure solid adenocarcinoma [28]. Some researchers have demonstrated that VPI negatively influences T1-sized pure solid tumors but not part solid tumors. They further proposed that the upgrade in the T stage due to VPI in T1-sized lung cancer may be suitable only for pure solid tumors [22, 23]. Unlike previous studies on VPI prediction using the radiomics method [27], our research objects were only T1-sized pure solid adenocarcinomas. The radiomics nomogram in our study achieved good predictive ability for VPI, indicating its clinical value.

Limitations

The present research has the following limitations. First, it is a retrospective study and divided the training and test cohorts according to the CT machines used, so that selection bias may exist. Second, this is a single-center study with a small sample size, so multi-center research with a larger sample size is needed to confirm the model reliability in the next step. Finally, all features were extracted from non-contrast enhanced chest imaging, and in future studies, contrast-enhanced CT imaging is needed to provide more information.

Conclusion

In summary, the CT-based radiomics nomogram can serve as a crucial reference for VPI prediction in T1-sized solid lung adenocarcinoma and may be used to guide clinical treatment decisions.

Acknowledgements

This work was supported by National Natural Science Foundation of China (No. 81671654 and No. 81571636), Taishan scholars of Shandong Province, China (No. tsqn202103197) and Shandong Province Natural Science Foundation (ZR2022MH274).

Disclosure of conflict of interest

None.

Address correspondence to: Heng Ma, Department of Radiology, Yantai Yuhuangding Hospital, Qingdao University School of Medicine, No. 20, Yudong Road, Zhifu District, Yantai 264001, Shandong, China. Tel: +86-13869360478; E-mail: mhytyhd@163.com

References

[1] Molina JR, Yang P, Cassivi SD, Schild SE and Adjei AA. Non-small cell lung cancer: epidemiology, risk factors, treatment, and survivorship. Mayo Clin Proc 2008; 83: 584-594.

[2] Chang YL, Lin MW, Shih JY, Wu CT and Lee YC. The significance of visceral pleural surface invasion in 321 cases of non-small cell lung cancers with pleural retraction. Ann Surg Oncol 2012; 19: 3057-3064.

[3] Dziedzic DA, Rudzinski P, Langfort R and Orlowski T; Polish Lung Cancer Study Group (PLCSG). Risk factors for local and distant recurrence after surgical treatment in patients with non-small-cell lung cancer. Clin Lung Cancer 2016; 17: e157-e167.

[4] Kudo Y, Saji H, Shimada Y, Nomura M, Matsubayashi J, Nagao T, Kakihana M, Usuda J, Kajiwara N, Ohira T and Ikeda N. Impact of visceral pleural invasion on the survival of patients with non-small cell lung cancer. Lung Cancer 2012; 78: 153-160.

[5] Liu A, Hou F, Qin Y, Song G, Xie B, Xu J and Jiao W. Predictive value of a prognostic model based on pathologic features in lung invasive adenocarcinoma. Lung Cancer 2019; 131: 14-22.

[6] Wo Y, Zhao Y, Qiu T, Li S, Wang Y, Lu T, Qin Y, Song G, Miao S, Sun X, Liu A, Kong D, Dong Y, Leng X, Du W and Jiao W. Impact of visceral pleural invasion on the association of extent of lymphadenectomy and survival in stage I non-small cell lung cancer. Cancer Med 2019; 8: 669-678.

[7] Yu Y, Huang R, Wang P, Wang S, Ling X, Zhang P, Yu J, Wang J, Xiao J and Wang Z. Sublobectomy versus lobectomy for long-term survival outcomes of early-stage non-small cell lung cancer with a tumor size ≤ 2 cm accompanied by visceral pleural invasion: a SEER population-based study. J Thorac Dis 2020; 12: 592-604.

[8] Yang Y, Xie Z, Hu H, Yang G, Zhu X, Yang D, Niu Z, Mao G, Shao M and Wang J. Using CT imaging features to predict visceral pleural invasion of non-small-cell lung cancer. Clin Radiol 2023; 78: e909-e917.

[9] Ahn SY, Park CM, Jeon YK, Kim H, Lee JH, Hwang EJ and Goo JM. Predictive CT features of visceral pleural invasion by T1-sized peripheral pulmonary adenocarcinomas manifesting as subsolid nodules. AJR Am J Roentgenol 2017; 209: 561-566.

[10] Deng HY, Li G, Luo J, Alai G, Zhuo ZG and Lin YD. Novel biologic factors correlated to visceral pleural invasion in early-stage non-small cell lung cancer less than 3 cm. J Thorac Dis 2018; 10: 2357-2364.

[11] Hsu JS, Han IT, Tsai TH, Lin SF, Jaw TS, Liu GC, Chou SH, Chong IW and Chen CY. Pleural tags on CT scans to predict visceral pleural invasion of non-small cell lung cancer that does not abut the pleura. Radiology 2016; 279: 590-596.

[12] Iizuka S, Kawase A, Oiwa H, Ema T, Shiiya N and Funai K. A risk scoring system for predicting visceral pleural invasion in non-small lung cancer patients. Gen Thorac Cardiovasc Surg 2019; 67: 876-879.

[13] Qi LP, Li XT, Yang Y, Chen JF, Wang J, Chen ML and Sun YS. Multivariate analysis of pleural in-

vasion of peripheral non-small cell lung cancer-based computed tomography features. J Comput Assist Tomogr 2016; 40: 757-762.
[14] Lambin P, Rios-Velazquez E, Leijenaar R, Carvalho S, van Stiphout RG, Granton P, Zegers CM, Gillies R, Boellard R, Dekker A and Aerts HJ. Radiomics: extracting more information from medical images using advanced feature analysis. Eur J Cancer 2012; 48: 441-446.
[15] Park S, Lee SM, Noh HN, Hwang HJ, Kim S, Do KH and Seo JB. Differentiation of predominant subtypes of lung adenocarcinoma using a quantitative radiomics approach on CT. Eur Radiol 2020; 30: 4883-4892.
[16] She Y, Zhang L, Zhu H, Dai C, Xie D, Xie H, Zhang W, Zhao L, Zou L, Fei K, Sun X and Chen C. The predictive value of CT-based radiomics in differentiating indolent from invasive lung adenocarcinoma in patients with pulmonary nodules. Eur Radiol 2018; 28: 5121-5128.
[17] Zuo Z, Li Y, Peng K, Li X, Tan Q, Mo Y, Lan Y, Zeng W and Qi W. CT texture analysis-based nomogram for the preoperative prediction of visceral pleural invasion in cT1N0M0 lung adenocarcinoma: an external validation cohort study. Clin Radiol 2022; 77: e215-e221.
[18] Wei SH, Zhang JM, Shi B, Gao F, Zhang ZX and Qian LT. The value of CT radiomics features to predict visceral pleural invasion in ≤ 3 cm peripheral type early non-small cell lung cancer. J Xray Sci Technol 2022; 30: 1115-1126.
[19] Siegel RL, Miller KD, Wagle NS and Jemal A. Cancer statistics, 2023. CA Cancer J Clin 2023; 73: 17-48.
[20] Zhao Q, Wang JW, Yang L, Xue LY and Lu WW. CT diagnosis of pleural and stromal invasion in malignant subpleural pure ground-glass nodules: an exploratory study. Eur Radiol 2019; 29: 279-286.
[21] Heidinger BH, Schwarz-Nemec U, Anderson KR, de Margerie-Mellon C, Monteiro Filho AC, Chen Y, Mayerhoefer ME, VanderLaan PA and Bankier AA. Visceral pleural invasion in pulmonary adenocarcinoma: differences in CT patterns between solid and subsolid cancers. Radiol Cardiothorac Imaging 2019; 1: e190071.
[22] Fu F, Zhang Y, Wen Z, Zheng D, Gao Z, Han H, Deng L, Wang S, Liu Q, Li Y, Shen L, Shen X, Zhao Y, Zhao Z, Ye T, Xiang J, Zhang Y, Sun Y, Hu H and Chen H. Distinct prognostic factors in patients with stage I non-small cell lung cancer with radiologic part-solid or solid lesions. J Thorac Oncol 2019; 14: 2133-2142.
[23] Okada S, Hattori A, Matsunaga T, Takamochi K, Oh S, Inoue M and Suzuki K. Prognostic value of visceral pleural invasion in pure-solid and part-solid lung cancer patients. Gen Thorac Cardiovasc Surg 2021; 69: 303-310.
[24] Rimner A, Ruffini E, Cilento V, Goren E, Ahmad U, Appel S, Bille A, Boubia S, Brambilla C, Cangir AK, Detterbeck F, Falkson C, Fang W, Filosso PL, Giaccone G, Girard N, Guerrera F, Huang J, Infante M, Kim DK, Lucchi M, Marino M, Marom EM, Nicholson AG, Okumura M, Rami-Porta R, Simone CB 2nd and Asamura H; Members of the IASLC Staging and Prognostic Factors Committee and of the Advisory Boards, and Participating Institutions. The international association for the study of lung cancer thymic epithelial tumors staging project: an overview of the central database informing revision of the forthcoming (ninth) edition of the TNM classification of malignant tumors. J Thorac Oncol 2023; 18: 1386-1398.
[25] Travis WD, Brambilla E, Rami-Porta R, Vallières E, Tsuboi M, Rusch V and Goldstraw P; International Staging Committee. Visceral pleural invasion: pathologic criteria and use of elastic stains: proposal for the 7th edition of the TNM classification for lung cancer. J Thorac Oncol 2008; 3: 1384-1390.
[26] Wang B, Sun K, Meng X, Bhuva MS, Sun X and Sun Y. The different evaluative significance of enlarged lymph nodes on preoperative CT in the N stage for patients with suspected subsolid and solid lung cancers. Acad Radiol 2023; 30: 1392-1399.
[27] Zha X, Liu Y, Ping X, Bao J, Wu Q, Hu S and Hu C. A nomogram combined radiomics and clinical features as imaging biomarkers for prediction of visceral pleural invasion in lung adenocarcinoma. Front Oncol 2022; 12: 876264.
[28] Hattori A, Matsunaga T, Takamochi K, Oh S and Suzuki K. Importance of ground glass opacity component in clinical stage IA radiologic invasive lung cancer. Ann Thorac Surg 2017; 104: 313-320.

Supplementary File 1. TRIPOD checklist

Section/Topic	Item		Checklist Item	Page
Title and abstract				
Title	1	D; V	CT-Based Radiomics Nomogram for Predicting Visceral Pleural Invasion in Peripheral T1-Sized Solid Lung Adenocarcinoma.	1
Abstract	2	D; V	This study aims to develop and validate a CT-based radiomics nomogram to predict visceral pleural invasion (VPI) in peripheral T1-sized solid lung adenocarcinoma. A total of 203 patients were selected as subjects and they were divided into training cohort and test cohort. The former was used to build the model and the latter was used to validate the model. Three models (clinical model, radscore and radiomics nomogram) were structured and their property was tested by their area under the curve (AUC). The nomogram showed higher classification property with an AUC of 0.877 (95% CI: 0.820-0.935) and 0.837 (95% CI: 0.737-0.937) in the training and test cohorts, respectively. In conclusion, The CT-based radiomics nomogram was useful for predicting VPI in peripheral T1-sized solid lung adenocarcinoma.	1-2
Introduction				
Background and objectives	3a	D; V	The preoperative assessment of VPI in patients with early lung adenocarcinoma is important. However, the diagnostic efficiency of VPI based on conventional CT features and clinical factors is not high. Radiomics is extensively applied in the diagnosis, pathological subtype classification, and prognosis prediction of lung cancer. However, a few studies focused on VPI in solid lung adenocarcinoma.	2-3
	3b	D; V	This study aims to develop and validate a CT-based radiomics nomogram to predict VPI in peripheral T1-sized solid lung adenocarcinoma.	3
Methods				
Source of data	4a	D; V	This is a retrospective study. All patients were collected from Yantai Yuhuangding Hospital.	3
	4b	D; V	From May 2019 to Feb 2021.	4
Participants	5a	D; V	A single-center diagnostic study.	4
	5b	D; V	Inclusion criteria: (1) adenocarcinoma, (2) distinct VPI status by pathology, (3) pure solid tumor on CT, (4) the largest diameter ≤ 3.0 cm, (5) peripheral lung cancer, (6) operation within two weeks after CT scan, and (7) complete medical records. Exclusion criteria: (1) neoadjuvant treatment history, (2) poor imaging quality.	4
	5c	D; V	-	
Outcome	6a	D; V	Whether the tumor produces VPI or not.	5-6
	6b	D; V	AUCs were calculated to assess each model property.	6
Predictors	7a	D; V	Clinical factors (extracted from medical records), conventional CT features (extracted from CT imaging by radiologist), radiomics characteristics (extracted from original CT imaging by the RadCloud platform).	4-5
	7b	D; V	Two radiologists who were unaware of the pathological findings assessed the conventional CT features of each case.	5
Sample size	8	D; V	The sample size was calculated with PASS software.	6
Missing data	9	D; V	-	6
Statistical analysis methods	10a	D	Kappa statistics and ICC were applied to measure the data consistency evaluation.	6
	10b	D	Univariate analysis and multivariate logistic regression analysis were performed to determine the independent risk factors in the training cohort to structure prediction models. The test cohort was used to validate the model.	6
	10c	V	Predictions were calculated by the nomogram.	6
	10d	D; V	The receiver operating characteristic (ROC) curve used to assess model performance and Delong test used to compare the performance of multiple models.	6
	10e	V	-	6
Risk groups	11	D; V	-	

Development vs. validation	12	V	There was no differences between the training and test cohorts in setting, eligibility criteria, outcome, and predictors.	6
Results				
Participants	13a	D; V	Flow chart for details (**Figure 2**).	6-7
	13b	D; V	In 203 cases, 55 cases (27.1%) were confirmed as VPI positive, and 148 cases (72.9%) were confirmed as VPI negative. Detailed clinical, CT, and radiomics features in **Table 1**.	6-7
	13c	V	There was no differences between the training and test cohorts of the distribution of important variables.	6
Model development	14a	D	Patients in training cohorts (N=141) were analysed to develop model. 38 cases (27.0%) were confirmed as VPI positive, and 103 cases (73.0%) were confirmed as VPI negative.	7
	14b	D	-	
Model specification	15a	D	Personalized prediction nomogram in **Figure 5**.	7
	15b	D	The score of variables were summed to obtain a total score for the VPI probability.	7
Model performance	16	D; V	The AUCs of nomogram were 0.877 and 0.837 in the training and test cohorts, respectively.	7-8
Model-updating	17	V	-	
Discussion				
Limitations	18	D; V	Retrospective study, single-center study, non-contrast enhanced imaging features.	10
Interpretation	19a	V	The radiomics nomogram achieved good VPI predictive ability with AUC of 0.837 in the validation cohort.	8
	19b	D; V	The radiomics nomogram achieved good predictive ability for VPI in T1-sized solid adenocarcinoma, and multi-center studies with large samples are needed to confirm the reliability of the model in the next step.	8
Implications	20	D; V	The radiomics nomogram model can assist preoperative evaluation of VPI in T1-sized pure solid adenocarcinoma and guided treatment decisions.	9-10
Other information				
Supplementary information	21	D; V	-	
Funding	22	D; V	National Natural Science Foundation of China (No. 81671654 and No. 81571636), Taishan scholars of Shandong Province, China (No. tsqn202103197) and Shandong Province Natural Science Foundation (ZR2022MH274).	1

Supplementary File 2. Rad score

Radscore =-0.032* wavelet-HHL_glrlm_ShortRunLowGrayLevelEmphasis + 0.027* wavelet-HLL_glrlm_RunVariance + 0.044* lbp-2D_firstorder_Median + 0.005* wavelet-LHL_glszm_SmallAreaHighGrayLevelEmphasis + -0.024* wavelet-LHL_glszm_LowGrayLevelZoneEmphasis + -0.001* wavelet-LHL_glszm_GrayLevelVariance + -0.011* wavelet-HLL_firstorder_Skewness + 0.014* original_glszm_SmallAreaHighGrayLevelEmphasis + -0.002* wavelet-LHL_firstorder_Skewness + 0.016* wavelet-HLL_ngtdm_Busyness + -0.009* wavelet-HLH_glszm_LowGrayLevelZoneEmphasis.